Thermoelectric and thermal rectification properties of quantum dot junctions

David M.-T. Kuo[1,2,*] and Yia-chung Chang[3,†]
[1]*Department of Electrical Engineering, National Central University, Chungli 320, Taiwan*
[2]*Department of Physics, National Central University, Chungli 320, Taiwan*
[3]*Research Center for Applied Sciences, Academia Sinica, Taipei 115, Taiwan*
(Received 25 February 2010; revised manuscript received 25 April 2010; published 26 May 2010)

The electrical conductance, thermal conductance, thermal power, and figure of merit (ZT) of semiconductor quantum dots (QDs) embedded into an insulator matrix connected with metallic electrodes are theoretically investigated in the Coulomb blockade regime. The multilevel Anderson model is used to simulate the multiple QDs junction system. The charge and heat currents in the sequential tunneling process are calculated by the Keldysh Green's function technique. In the linear-response regime the ZT values are still very impressive in the small tunneling rates case, although the effect of electron Coulomb interaction on ZT is significant. In the nonlinear-response regime, we have demonstrated that the thermal rectification behavior can be observed for the coupled QDs system, where the very strong asymmetrical coupling between the dots and electrodes, large energy-level separation between dots and strong interdot Coulomb interactions are required.

DOI: 10.1103/PhysRevB.81.205321 PACS number(s): 65.80.−g, 73.50.Lw, 73.63.Kv

I. INTRODUCTION

Due to energy and environment issues, it becomes important to consider novel applications related to the thermal properties of materials. Recently, many efforts have been devoted to seeking efficient thermoelectric materials because there exist potential applications of solid-state thermal devices.[1–9] Nevertheless, the optimization of thermoelectric properties of materials is extremely difficult, since the figure of merit ($ZT=S^2G_eT/\kappa$) depends on the Seebeck coefficient (S), electrical conductance (G_e), and thermal conductance (κ) of the material. Tuning one of these physical quantities will unavoidably alter others because they are closely related.[7]

Several methods were proposed to realize the enhancement of ZT.[2] One of them is to reduce the system dimensionality.[8] Bi_2Te_3/Sb_2Te_3 superlattices,[3] silicon quantum wires,[4] and PbSeTe-based quantum dot (QD) superlattices[5] were experimentally demonstrated to show much higher ZT values when compared with their corresponding bulk materials. A zero-dimensional QD system was predicted to have more pronounced enhancement in thermoelectric efficiency due the reduced dimensionality.[9] Experimentally, it has been shown[5] that the performance of PbSeTe QDs can reach a very impressive ZT value of 2. Nevertheless, a ZT value higher than 3 has never been reported. Note that the highest ZT value is near 1 for conventional bulk materials.[1] Systems with ZT value larger than 3 may find application in making home refrigerators, replacing the existing compressor-based refrigerators. In addition, they can be used in electrical power generators.[2]

In order to seek a large ZT value, a single-molecular QD weakly linked to electrodes was proposed to exhibit an extremely large ZT value in the Coulomb-blockade regime.[10] However, Ref. 10 did not take into account the molecular vibrations. For a molecular junction, the coupling strengths between localized electrons and vibration modes are very strong.[11–17] Due to multiple-phonon-assisted processes arising from strong electron-phonon interactions, it is expected that ZT values will be suppressed by molecular vibrations. Apart from that, such a molecular junction is difficult to integrate with current silicon-based electronics. Therefore, we propose to use a thermoelectric device made of semiconductor QDs embedded into amorphous insulator (e.g., SiO_2) which has low heat conductivity. Heat is a waste and degrades electronic device performance, so removing heat in semiconductor device and integrated circuit (IC) is a major problem in the huge IC industry. The proposed Si/SiO_2 QDs can be fabricated using complementary metal-oxide-semiconductor compatible processes. A schematic of the proposed system is shown in Fig. 1. A nanoscale vacuum layer is inserted to block the heat current delivered by phonon carriers, although it would be a challenging task to keep the vacuum layer thin enough to allow sufficient electron tunneling. As we shall explain below, the presence of a vacuum layer is essential for optimizing the ZT value and the thermal rectification for the QD junction device. The vacuum layer considered here could be realized by first depositing a nanoscale photoresist layer on top of the Si/SiO_2 QD layer, selectively etching out a few pinholes on the photoresist, and then depositing a metallic contact layer on top of the photoresist. Finally, use chemical etching to remove all the photoresist between the metal contact layer and the Si/SiO_2 QD layer, leaving an air gap in between. The metallic material that enters the pinholes will remain as the nanopillar support to keep the metallic overlayer from collapsing down to the QD layer. (See steps 1–4 as illustrated in Fig. 1.) Once the nanoscale air gap is formed, removing the air to make a high-vacuum layer can be done by using the technology similar to that used in liquid-crystal display implementation where a vacuum layer is inserted for blocking the heat generated by the light source.

The key applications of thermoelectric devices include solid-state refrigerators and electrical generators. In solid-state refrigerators (electrical generators), one needs to remove (generate) large amount of heat current (charge current). Consequently, a high-QD density is required for realistic applications. A single-level Anderson model can be used to simulate such a system adequately in the dilute QD-

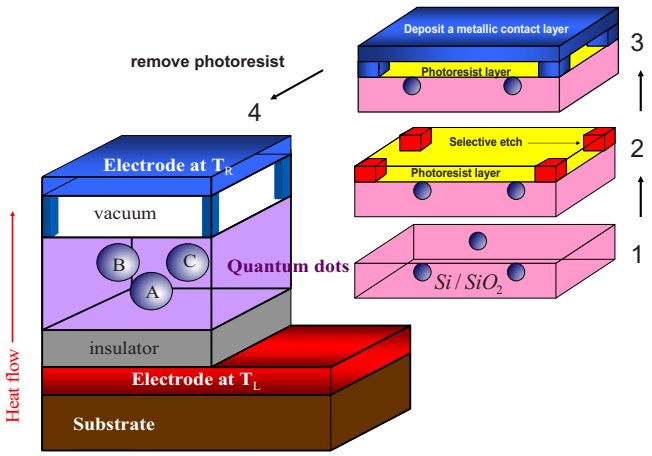

FIG. 1. (Color online) Schematic of the IQV tunnel junction device. Four processing steps are needed to achieve this: (1) depositing a nanoscale photoresist layer on top of the Si/SiO_2 QD layer, (2) selectively etch out a few pinholes on the photoresist, (3) deposit a metallic contact layer on top of the photoresist, and (4) use chemical etching to remove all the photoresist between the metal contact layer and the Si/SiO_2 QD layer, leaving an air gap in between.

density limit.[10] However, for the high-QD-density system, one needs to consider the effect of interdot Coulomb interactions and electron hopping effect. When QDs are embedded in an insulator matrix having a high-potential barrier, electron hopping among dots can be neglected. However, it is hard to avoid the interdot Coulomb interactions due to its long-range tail.

In this paper, we investigate the effect of interdot Coulomb interactions on the thermoelectric properties in the linear- and nonlinear-response regimes via a multilevel Anderson model.[18,19] We found that the interdot Coulomb interactions would suppress the ZT values and play a crucial role in determining the thermal rectification behavior. The electrical conductivity, thermal power, thermal conductivity, and figure of merit were typically calculated in the linear-response regime, while crucial applications of thermal devices in thermal rectifiers and transistors require the understanding of the thermoelectric properties in the nonlinear-response regime.[20,21] The thermal rectifiers can be used in solar-energy storage and many other applications. Therefore, it is important to take into account the thermoelectric effects in the nonlinear regime. Here, we demonstrate that coupled QDs can exhibit pronounced thermal rectification behavior. Although the mechanism of thermal rectification for QD junctions is similar to that of charge current, the heat current is generated by temperature gradient and the consequent electrochemical potential. It is the nonlinear relation for the electrical/thermal current as a function of the applied temperature and electrochemical-potential gradients that leads to enhance thermal rectification behavior.

II. FORMALISM

A schematic of the system of concern is shown in Fig. 1. The Hamiltonian of the system can be described by a multilevel Anderson model

$$H = \sum_{k,\sigma,\beta} \epsilon_k a^\dagger_{k,\sigma,\beta} a_{k,\sigma,\beta} + \sum_{\ell,\sigma} E_\ell d^\dagger_{\ell,\sigma} d_{\ell,\sigma} + \sum_{\ell,\sigma} U_\ell d^\dagger_{\ell,\sigma} d_{\ell,\sigma} d^\dagger_{\ell,-\sigma} d_{\ell,-\sigma} + \frac{1}{2} \sum_{\ell \neq j;\sigma,\sigma'} U_{\ell,j} d^\dagger_{\ell,\sigma} d_{\ell,\sigma} d^\dagger_{j,\sigma'} d_{j,\sigma'} + \sum_{k,\sigma,\beta,\ell} V_{k,\beta,\ell} a^\dagger_{k,\sigma,\beta} d_{\ell,\sigma} + \sum_{k,\sigma,\beta,\ell} V^*_{k,\beta,\ell} d^\dagger_{\ell,\sigma} a_{k,\sigma,\beta}, \quad (1)$$

where $a^\dagger_{k,\sigma,\beta}$ ($a_{k,\sigma,\beta}$) creates (destroys) an electron of momentum k and spin σ with energy ϵ_k in the β metallic electrode. $d^\dagger_{\ell,\sigma}$ ($d_{\ell,\sigma}$) creates (destroys) an electron with the ground-state energy E_ℓ in the ℓth QD, U_ℓ and $U_{\ell,j}$ describe the intradot Coulomb interactions and the interdot Coulomb interactions, respectively. $V_{k,\beta,\ell}$ describes the coupling between the band states of electrodes and the QD levels. We have ignored the excited levels of QDs, assuming that the energy-level separation between the ground state and the first excited state within each QD is much larger than the thermal energy k_BT, where T is the temperature of concern. We have also ignored the inderdot hopping terms due to the high-potential barrier of the insulating material (e.g., SiO_2) separating QDs. The key effects included are intradot and interdot Coulomb interactions and the coupling between the QDs with the metallic leads.

Using the Keldysh-Green's function technique,[22,23] charge and heat currents leaving electrodes can be expressed as

$$J_e = \frac{-2e}{h} \sum_\ell \int d\epsilon \gamma_\ell(\epsilon) \mathrm{Im}\, G^r_{\ell,\sigma}(\epsilon) f_{LR}(\epsilon), \quad (2)$$

$$Q = \frac{-2}{h} \sum_\ell \int d\epsilon \gamma_\ell(\epsilon) \mathrm{Im}\, G^r_{\ell,\sigma}(\epsilon)(\epsilon - E_F - e\Delta V) f_{LR}(\epsilon), \quad (3)$$

where the transmission factor is $\gamma_\ell(\epsilon) = \frac{\Gamma_{\ell,L}(\epsilon)\Gamma_{\ell,R}(\epsilon)}{\Gamma_{\ell,L}(\epsilon)+\Gamma_{\ell,R}(\epsilon)}$. $f_{LR}(\epsilon) = f_L(\epsilon) - f_R(\epsilon)$, where $f_{L(R)}(\epsilon) = 1/[e^{(\epsilon-\mu_{L(R)})/k_BT_{L(R)}}+1]$ is the Fermi distribution functions for the left (right) electrode. The chemical-potential difference between these two electrodes is related to the bias difference via $\mu_L - \mu_R = e\Delta V$. E_F is the Fermi energy of electrodes. $\Gamma_{\ell,L}(\epsilon)$ and $\Gamma_{\ell,R}(\epsilon)$ [$\Gamma_{\ell,\beta} = 2\pi\Sigma_{\mathbf{k}}|V_{\ell,\beta,\mathbf{k}}|^2\delta(\epsilon - \epsilon_{\mathbf{k}})$] denote the tunneling rates from the QDs to left and right electrodes, respectively. e and h denote the electron charge and Plank's constant, respectively. For simplicity, these tunneling rates will be assumed energy and bias independent. Therefore, the calculation of tunneling current and heat current is entirely determined by the spectral function, $A(\epsilon) = \mathrm{Im}\, G^r_{\ell,\sigma}(\epsilon)$, which is the imaginary part of the retarded Green's function $G^r_{\ell,\sigma}(\epsilon)$. The expression of retarded Green's function is given by[18,19]

$$G^r_{\ell,\sigma}(\epsilon) = (1 - N_{\ell,-\sigma}) \sum_{m=1}^{3^{n-1}} \frac{p_m}{\epsilon - E_\ell - \Pi_m + i\Gamma_\ell} + N_{\ell,-\sigma} \sum_{m=1}^{3^{n-1}} \frac{p_m}{\epsilon - E_\ell - U_\ell - \Pi_m + i\Gamma_\ell}, \quad (4)$$

where n denotes the number of coupled QDs in each cell considered. Π_m denotes the sum of Coulomb interactions seen by a particle in dot ℓ due to other particles in the dot $j(j \neq \ell)$, which can be occupied by zero, one or two particles. p_m denotes the probability of such configurations. For a three-QD cell ($\ell \neq j \neq j'$), there are nine (3×3) configurations, and the probability factors become $p_1 = a_j a_{j'}$, $p_2 = b_j a_{j'}$, $p_3 = a_j b_{j'}$, $p_4 = c_j a_{j'}$, $p_5 = c_{j'} a_j$, $p_6 = b_j b_{j'}$, $p_7 = c_j b_{j'}$, $p_8 = c_{j'} b_j$, and $p_9 = c_j c_{j'}$, where $a_j = 1 - (N_{j,\sigma} + N_{j,-\sigma}) + c_j$, $b_j = (N_{j,\sigma} + N_{j,-\sigma}) - 2c_j$, and $c_j = \langle n_{j,-\sigma} n_{j,\sigma} \rangle$ is the intradot two-particle correlation function. $N_{j,\sigma}$ is one-particle occupation number. Interdot Coulomb interaction factors are $\Pi_1 = 0$, $\Pi_2 = U_{\ell,j}$, $\Pi_3 = U_{\ell,j'}$, $\Pi_4 = 2U_{\ell,j}$, $\Pi_5 = 2U_{\ell,j'}$, $\Pi_6 = U_{\ell,j} + U_{\ell,j'}$, $\Pi_7 = 2U_{\ell,j} + U_{\ell,j'}$, $\Pi_8 = 2U_{\ell,j'} + U_{\ell,j}$, and $\Pi_9 = 2U_{\ell,j} + 2U_{\ell,j'}$. $\Gamma_\ell = (\Gamma_{\ell,L} + \Gamma_{\ell,R})/2$ arises from the self-energy due to the weak coupling between the QDs with metallic leads, where the real part of self-energy is ignored. Such a self-energy (ignoring the effect of electron Coulomb interactions) is adequate within the Coulomb-blockade regime, but it does not capture the Kondo effect. The sum of probability factors p_m for all configurations is equal to 1, reflecting the fact that $G^r_{\ell,\sigma}(\epsilon)$ satisfies the sum rule.

According to the expression of retarded Green's function of Eq. (4), we need to know the single-particle and two-particle occupation numbers, $N_{\ell,\sigma}(N_{\ell,-\sigma})$ and $N_{\ell,\ell} = c_\ell$, which can be obtained by solving the following equations self-consistently:

$$N_{\ell,\sigma} = -\int \frac{d\epsilon}{\pi} \frac{\Gamma_{\ell,L} f_L(\epsilon) + \Gamma_{\ell,R} f_R(\epsilon)}{\Gamma_{\ell,L} + \Gamma_{\ell,R}} \mathrm{Im}\, G^r_{\ell,\sigma}(\epsilon), \quad (5)$$

$$c_\ell = -\int \frac{d\epsilon}{\pi} \frac{\Gamma_{\ell,L} f_L(\epsilon) + \Gamma_{\ell,R} f_R(\epsilon)}{\Gamma_{\ell,L} + \Gamma_{\ell,R}} \mathrm{Im}\, G^r_{\ell,\ell}(\epsilon). \quad (6)$$

The values of $N_{\ell,\sigma}$ and c_ℓ are restricted between 0 and 1. The expression of two-particle-retarded Green's function of Eq. (6) is

$$G^r_{\ell,\ell}(\epsilon) = N_{\ell,-\sigma} \sum_{m=1}^{3^{n-1}} \frac{p_m}{\epsilon - E_\ell - U_\ell - \Pi_m + i\Gamma_\ell}.$$

III. LINEAR-RESPONSE REGIME

In the linear-response regime, Eqs. (2) and (3) can be rewritten as

$$J_e = \mathcal{L}_{11} \frac{\Delta V}{T} + \mathcal{L}_{12} \frac{\Delta T}{T^2},$$

$$Q = \mathcal{L}_{21} \frac{\Delta V}{T} + \mathcal{L}_{22} \frac{\Delta T}{T^2}, \quad (7)$$

where $\Delta T = T_L - T_R$ is the temperature difference across the junction. Coefficients in Eq. (7) are given by

$$\mathcal{L}_{11} = \frac{2e^2 T}{h} \int d\epsilon \mathcal{T}(\epsilon) \left(\frac{\partial f(\epsilon)}{\partial E_F} \right)_T, \quad (8)$$

$$\mathcal{L}_{12} = \frac{2eT^2}{h} \int d\epsilon \mathcal{T}(\epsilon) \left(\frac{\partial f(\epsilon)}{\partial T} \right)_{E_F}, \quad (9)$$

$$\mathcal{L}_{21} = \frac{2eT}{h} \int d\epsilon \mathcal{T}(\epsilon)(\epsilon - E_F) \left(\frac{\partial f(\epsilon)}{\partial E_F} \right)_T, \quad (10)$$

and

$$\mathcal{L}_{22} = \frac{2T^2}{h} \int d\epsilon \mathcal{T}(\epsilon)(\epsilon - E_F) \left(\frac{\partial f(\epsilon)}{\partial T} \right)_{E_F}. \quad (11)$$

Here $\mathcal{T}(\epsilon) = -\sum_\ell \frac{\Gamma_{\ell,L}(\epsilon)\Gamma_{\ell,R}(\epsilon)}{\Gamma_{\ell,L}(\epsilon) + \Gamma_{\ell,R}(\epsilon)} \mathrm{Im}\, G^r_{\ell,\sigma}(\epsilon)|_{\Delta V = 0, \Delta T = 0}$ and $f(\epsilon) = 1/[e^{(\epsilon - E_F)/k_B T} + 1]$. Note that the Onsager relation $\mathcal{L}_{12} = \mathcal{L}_{21}$ is preserved. Based on Eq. (7), the charge current can be generated by the voltage difference and temperature gradient. If the system is in an open circuit, the electrochemical potential will form in response to a temperature gradient; this electrochemical potential is known as the Seebeck voltage (Seebeck effect). Seebeck coefficient (the amount of voltage generated per unit temperature gradient) is defined as $S = \frac{\Delta V}{\Delta T} = -\frac{1}{T} \frac{\mathcal{L}_{12}}{\mathcal{L}_{11}}$. In terms of the Seebeck coefficient, the electron thermal conductance is $\kappa_e = (\frac{\mathcal{L}_{22}}{T^2} - \mathcal{L}_{11} S^2)$. To judge whether the system is able to generate power or refrigerate efficiently, we need to evaluate the figure of merit, $ZT = S^2 G_e T/\kappa$, where $G_e = \frac{1}{T}\mathcal{L}_{11}$ is the electrical conductance and $\kappa = \kappa_e + \kappa_{ph}$ is the thermal conductance. κ_{ph} denotes the thermal conductance due to the phonon contribution. For a system with an efficient thermoelectric properties we want ZT as high as possible. This implies that we desire a system with high Seebeck coefficient, high electrical conductance, and low thermal conductance. The thermal conductance arising from phonons can be neglected ($\kappa = \kappa_e$) in our proposed system because the vacuum layer can block the heat current carried by phonons effectively.

Although Eq. (4) can be employed to calculate the charge current and heat current of a junction system with arbitrary QD number,[18,19] here we use the three-QD example to investigate the effect of interdot Coulomb interaction on the figure of merit, ZT. As mentioned above, ZT depends on the electrical conductance G_e, Seebeck coefficient S, and electron thermal conductance κ_e. Therefore, it is difficult to calculate the exact solution of ZT for arbitrary parameters. For simplicity, we have ignored the QD size fluctuations and assumed all QDs have the same ground-state energy, $E_\ell = E_g$ in the evaluation of ZT. The QD size fluctuations will become important in the consideration of heat-current rectification below. The closed form expressions for the coefficients de-

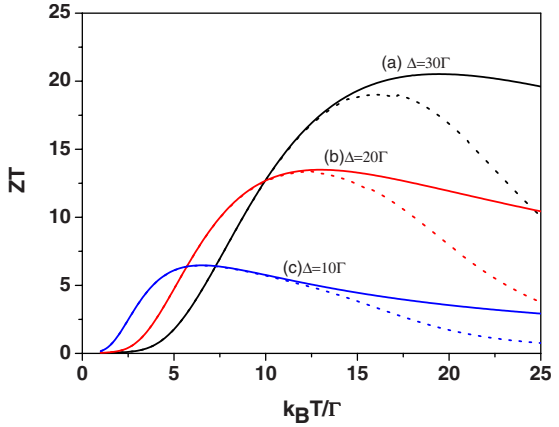

FIG. 2. (Color online) Figure of merit ZT as a function of temperature for various values of Δ in the absence of interdot Coulomb interactions. Solid lines and dotted lines correspond to $U=0$ and $U=125\Gamma$, respectively.

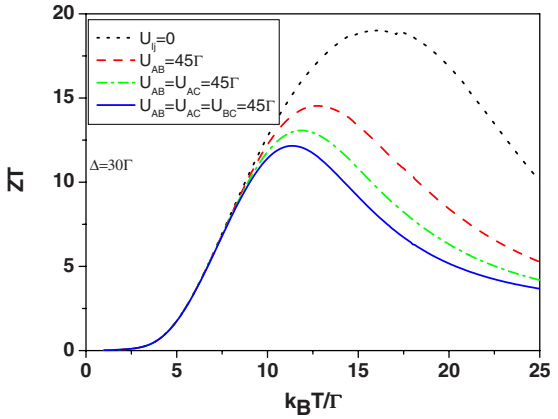

FIG. 3. (Color online) Figure of merit ZT as a function of temperature for various quantum dot configurations.

fined in Eqs. (8)–(11) exist within the small tunneling-rate limit [i.e., $\frac{\Gamma/2}{(\epsilon-E_g)^2+\Gamma^2/4}$ can be approximated by $\pi\delta(\epsilon-E_g)$] and no electron Coulomb interaction. We obtain

$$\mathcal{L}_{11} = \alpha_0/\cosh^2[\Delta/(2k_BT)],$$

$$\mathcal{L}_{12} = \mathcal{L}_{21} = \alpha_1/\cosh^2[\Delta/(2k_BT)],$$

and

$$\mathcal{L}_{22} = \alpha_2/\cosh^2[\Delta/(2k_BT)],$$

where $\Delta \equiv E_g - E_F$, $\alpha_0 = \frac{3e^2\pi}{2hk_B}\frac{\Gamma_L\Gamma_R}{\Gamma}$, $\alpha_1 = \frac{3e\pi}{2hk_B}\frac{\Gamma_L\Gamma_R}{\Gamma}\Delta$, and $\alpha_2 = \frac{3\pi}{2hk_B}\frac{\Gamma_L\Gamma_R}{\Gamma}\Delta^2$. We find that the thermal conductance $\kappa_e = (\frac{\mathcal{L}_{22}}{T^2} - \mathcal{L}_{11}S^2)$ vanishes whereas the electrical conductance of $G_e = \frac{1}{T}\mathcal{L}_{11}$ and the thermal power of $S = -\frac{1}{T}\frac{\mathcal{L}_{12}}{\mathcal{L}_{11}}$ remain finite. This indicates that system ZT diverges as Γ approaches zero. This is the so-called "Carnot efficiency."[10]

Closed-form expressions for these coefficients for finite Γ in the noninteracting case have also been derived in terms of trigamma functions.[10] However, the complicated trigamma functions do not simplify the expression of ZT and make it difficult to elucidate mechanisms for optimizing ZT. Therefore, we numerically calculate the figure of merit ZT with and without the Coulomb interactions. We first consider the case of symmetrical tunneling rates ($\Gamma_L = \Gamma_R = 1$ meV). The consideration of asymmetrical tunneling rates is not important for the linear-response regime, but it is crucial for the nonlinear regime,[20,21] which we shall address in the next section. ZT as a function of temperature for various values of Δ in the absence of interdot Coulomb interactions is shown in Fig. 2. Solid lines and dotted lines denote cases without and with intradot Coulomb interaction ($U=125\Gamma$), respectively. Note that all energies are measured in terms of Γ throughout this paper. We see that the solid lines merge with the dashed lines at low temperatures. This indicates that the effect of intradot Coulomb interaction on ZT can be ignored when $U \gg k_BT$. Such a result can be understood as follows. When interdot Coulomb interactions $U_{\ell,j} = U_{ds}$ vanish, the retarded Green's function consists of two branches

$$G_\ell^r(\epsilon) = \frac{1 - N_{\ell,\sigma}}{\epsilon - E_g + \Gamma} + \frac{N_{\ell,\sigma}}{\epsilon - E_g - U + \Gamma}. \quad (12)$$

The second branch has a negligible contribution due to the vanishing factor $\exp^{-(E_g+U-E_F)/k_BT}$ (when $U \gg k_BT$ and $\Delta > 0$) which appears in Eqs. (8)–(11). The factor $(1-N_{\ell,\sigma})$ in the first branch of Eq. (12) only affects the coefficients ($\mathcal{L}_{11}$, $\mathcal{L}_{12}$, $\mathcal{L}_{21}$, and $\mathcal{L}_{22}$), but not their ratios. This explains why $ZT(U=0) \approx ZT(U \gg k_BT)$. The reduction in ZT at finite U (for instance, $U/k_BT=5$) can be understood as follows. In the small tunneling-rate limit, we find that $S^2G_e \propto \Gamma$ and $\kappa_e \propto \Gamma$ for finite U. This is different from the behavior, $S^2G_e \propto \Gamma$ and $\kappa_e \propto \Gamma^2$ in the absence of U. Consequently, the reduction in ZT is observed in Fig. 2.

For a thermoelectric device with high-QD density, the interdot Coulomb interactions are also important. Figure 3 shows the ZT value as a function of temperature for a three-QD cell for various QD configurations with $\Delta=30$ Γ and $U=125$ Γ. Dotted line denotes the case of dilute QD density. As a result of a large separation between QDs, the interdot Coulomb interactions are negligible ($U_{\ell,j}=0$). Dashed lines denote the case where dot A and dot B are close to each other ($U_{AB}=45\Gamma$) but dot C is far from them ($U_{AC}=U_{BC}=0$). Dotted-dashed line denotes the case with $U_{AB}=U_{AC}=45\Gamma$ but $U_{BC}=0$. Solid line denotes the case with $U_{AB}=U_{AC}=U_{BC}=45\Gamma$. The results of Fig. 3 indicate considerable reduction in ZT at high temperatures due to the interdot Coulomb interactions (proximity effect). However, the proximity effect on ZT can be ignored when $U_{\ell,j}/k_BT \gg 1$. In general, the maximum values of interdot Coulomb interactions are one half of intradot Coulomb interactions. For silicon QDs embedded in SiO_2, the Si QDs with 5–10 nm diameters have the intradot Coulomb interaction strengths between 100–150 meV. Therefore, the condition of $U_{\ell,j}/k_BT \gg 1$ is not easy to be satisfied at room temperature.

According to the results of Fig. 2, the system ZT can be tuned by the Δ value. In Fig. 4, we plot ZT as a function of Δ for the three-QD system with Coulomb interactions for various temperatures. For comparison, we also plot the noninteracting case (dotted curve superposed on solid curve) at $k_BT=15\Gamma$, where the maximum ZT value occurred at Δ_{max}

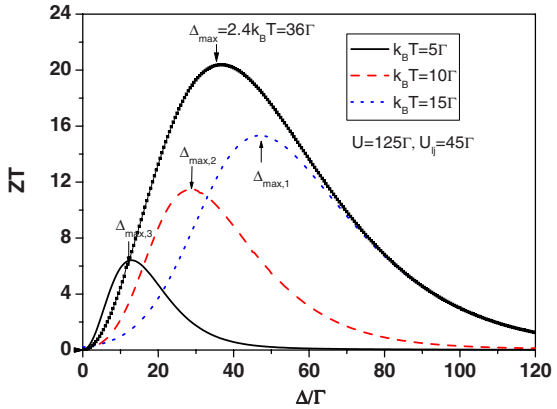

FIG. 4. (Color online) Figure of merit ZT as a function of Δ for three different temperatures for the case with interdot Coulomb interactions. The noninteracting case at $k_BT=15\Gamma$ (dotted curve superposed on solid curve) is also shown for comparison.

$=2.4k_BT$ as has been pointed out in Ref. 10. However, for the case with finite electron Coulomb interactions, we found $\Delta_{max,1}=3.1k_BT$, $\Delta_{max,2}=3k_BT$, and $\Delta_{max,3}=2.8k_BT$. It is worth noting that the maximum ZT values for different temperatures still reach $ZT_{max}\geq 3$, which are very encouraging values. However, we have not considered the QD size fluctuations, defects between metallic electrodes and insulators, and electron-phonon interactions. In order to include these affects fully, we phenomenologically replace the imaginary part of retarded Green's function of Eq. (4) by $\Gamma_\ell+\Gamma_{ie}$. This means the total level width is expressed as the sum of elastic and inelastic widths. Figure 5 shows the inelastic scattering effect on ZT. For $\Gamma_{ie}=3\Gamma$, the maximum ZT value becomes smaller than 4. The results of Fig. 5 indicate that the suppression of ZT_{max} resulting from the inelastic scattering is serious.

To further understand the results of Figs. 3 and 4, we analyze the electron conductance G_e, thermal power S, and electron thermal conductance κ_e of the system. Figure 6 shows G_e, S, and κ_e as functions of temperature for a three-QD cell for various configurations: $U_{AB}=U_{AC}=U_{BC}=45\Gamma$ (dotted curves), $U_{AB}=U_{AC}=45\Gamma$ and $U_{BC}=0$ (dashed curves), and $U_{AB}=45\Gamma$ and $U_{AC}=U_{BC}=0$ (solid curves), which correspond to strong-, medium-, and weak-proximity

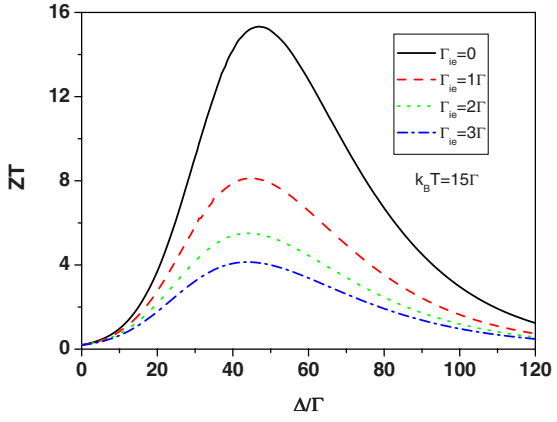

FIG. 5. (Color online) Figure of merit ZT as a function of Δ for various inelastic scattering strengths at $k_BT=15\Gamma$.

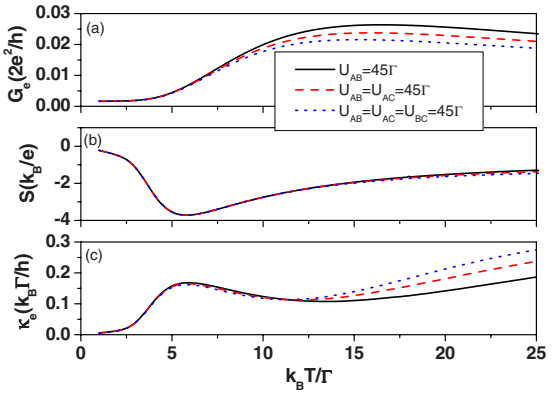

FIG. 6. (Color online) Electrical conductance G_e, thermal power S, and electron thermal conductance κ_e as a function of temperature for various quantum dot configurations.

effects. We noticed from Fig. 6(b) that the thermal power (S) is not sensitive to the proximity effect, which means the proximity effects on $\mathcal{L}_{12}$ and $\mathcal{L}_{11}$ are similar. Thus, the ZT behavior at high temperature shown in Fig. 3 is mainly attributed to κ_e and G_e. κ_e is enhanced [see Fig. 6(c)] but G_e is suppressed [see Fig. 6(a)] at high temperature when the proximity effect increases. This explains why ZT is suppressed at high temperature with increasing proximity effect. The maximum absolute value of S appears at near $k_BT=6\Gamma$, whereas the maximum ZT value shown in Fig. 3 appears between $k_BT=10\Gamma$ and $k_BT=15\Gamma$. So the temperature dependence of ZT is similar to that of the electrical conductance G_e, meaning that S^2T/κ_e has a weak temperature dependence.

In Fig. 4, we have tuned Δ from 0 to 120Γ. This implies that the energy levels of QDs are shifted away from the Fermi energy of electrodes. ZT becomes small when $\Delta/k_BT\gg 1$. We can apply a gate voltage (V_g) to move E_g relative to E_F. In Fig. 7 we plot G_e, S, and κ_e as functions of the gate voltage (V_g) for various temperatures with Δ fixed at 30Γ. The electric conductance (G_e) clearly exhibits a Coulomb oscillation arising from intradot and interdot Coulomb interactions. The first three peaks of G_e result from the reso-

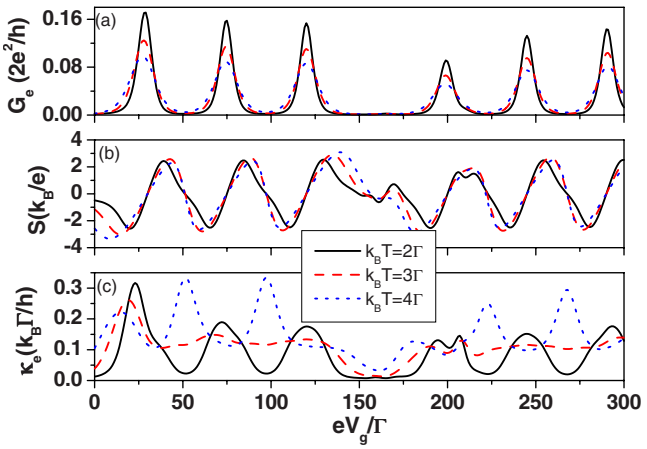

FIG. 7. (Color online) Electrical conductance G_e, thermal power S, and electron thermal conductance κ_e as a function of applied gate voltage for various temperatures at $\Delta=30\Gamma$, $U=125\Gamma$ and $U_{lj}=45\Gamma$.

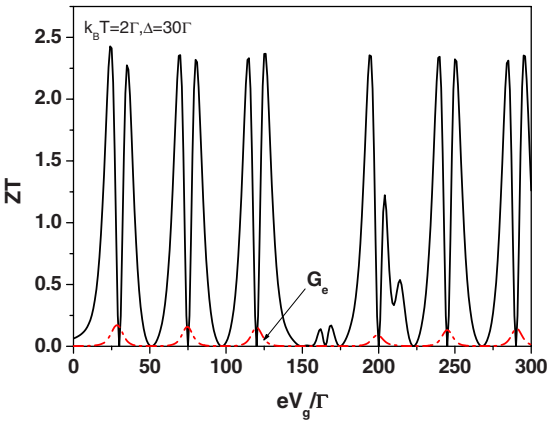

FIG. 8. (Color online) Figure of merit ZT as a function of applied gate voltage (solid curve) at $k_BT=2\Gamma$, $\Delta=30\Gamma$, $U=125\Gamma$ and $U_{lj}=45\Gamma$. The corresponding electrical conductance G_e (dotted-dashed curve) for comparison.

nant channels of poles at E_g, E_g+U_{ds}, and E_g+2U_{ds} for ϵ. Other peaks can be readily identified by the resonant channels of retarded Green's function of Eq. (4). Note that the resonant channel of $\epsilon=E_g+U$ $(=155\Gamma)$ is seriously suppressed due to the fact that all three QDs are filled with one electron at that gate voltage. The Coulomb oscillatory behavior of G_e becomes smeared at higher temperatures.

The thermal power (S) exhibits a sawtoothlike shape with respect to gate voltage, which is consistent with the experimental observation.[24] The sawtoothlike shape was also predicted theoretically in the metallic single-electron transistor,[25,26] where the charging energies are homogeneous. In Refs. 25 and 26, a model based on the rate equations was adopted. The thermal power S can be tuned from negative to positive values. When the Fermi energy matches a resonant channel (G_e reaches a maximum value), the thermal power vanishes, since $\mathcal{L}_{12}=0$. When the Fermi energy of electrodes is in the middle of two resonant channels, S also vanishes. Zero thermal power indicates that the current arising from temperature gradient can be self-consistently balanced without electrochemical potential. Note that the other interesting characteristics of thermal power of a single QD in the Kondo regime or cotunneling process have been experimentally and theoretically studied in Refs. 27 and 28. The behavior of κ_e is much more complicated than that of G_e, since $\kappa_e=(\frac{\mathcal{L}_{22}}{T^2}-\mathcal{L}_{11}S^2)$ which consists of $\mathcal{L}_{11}$, $\mathcal{L}_{12}$, and $\mathcal{L}_{22}$. Since κ_e is positive definite, we obtain the relation $\frac{\mathcal{L}_{22}}{T^2}\geq\mathcal{L}_{11}S^2$. When thermal power vanishes, $\kappa_e=\frac{\mathcal{L}_{22}}{T^2}$. Based on the results shown in Fig. 7, the optimized ZT value does not match either the maximum G_e (good conductor) or the minimum G_e (poor conductor). The largest value for ZT is obtained midway between good and poor conductors as illustrated in Fig. 8 for $k_BT=2\Gamma$ and $\Delta=30\Gamma$.

Before studying thermoelectric properties in the nonlinear regime, we briefly discuss the effects of phonon thermal conductance κ_{ph} and electron hopping between QDs on ZT values. Because the vacuum layer is considered, the phonon thermal conductance κ_{ph} can be neglected in the above calculations of ZT. Nevertheless, the implementation of vacuum layer without support is impossible. In our design, nanopillars are used to form a support for the vacuum space. Recently, experimental and theoretical works[4,29,30] have reported the serious suppression of κ_{ph} in nanowires. Therefore, if the surface density of nanopillars in the vacuum layer is N_p, then the thermal conductance per unit area of the nanopillar filled vacuum layer becomes $N_p\kappa_{ph}=N_p\kappa_{ph,0}F_s$, where $\kappa_{ph,0}=\frac{\pi^2k_B^2T}{3h}$ is the universal thermal conductance due to confined acoustic phonons[31] and F_s is the dimensionless parameter resulting from the surface scattering.[29,30] The calculated ZT for the whole device should be modified by $ZT=\frac{N_{\rm QD}S^2G_eT}{N_{\rm QD}\kappa_e+N_p\kappa_{ph}}=\frac{S^2G_eT}{\kappa_e(1+f\kappa_{ph}/\kappa_e)}$, where $N_{\rm QD}$ is number of QDs per unit area and $f=N_p/N_{\rm QD}$ is the ratio of surface density of nanopillars to that of quantum dots embedded in the QD layer, which shall be taken to be 0.01. Using the results of Fig. 6(c) as an example, the ratio of $f\kappa_{ph}/\kappa_e$ at $k_BT=10\Gamma$ is between 0.2 and 0.1 when we consider F_s between 0.1 and 0.05, which are adequate according to Refs. 29 and 30. This will only reduce the results of Fig. 3 by 10–20 %. However, if the entire vacuum layer is replaced by a good thermal insulator such as SiO_2, then the ratio f in the above should be replaced by a value larger than 1. This would lead to a value of $f\kappa_{ph}/\kappa_e>10$ and the ZT value will become less than 1.

Owing to the high-potential barrier separating each QD, the electron hopping terms among QDs have been ignored in the above studies. When the interdot hopping processes between QDs is included (details to be presented elsewhere), we have found that (for the case of two coupled dots) (a) the electrical conductance is enhanced, (b) the thermal power is not very sensitive to electron hopping terms, and (c) the electrical thermal conductance is enhanced faster than that of electrical conductance (when we assume the tunneling rate is the same as the decoupled case). Consequently, the maximum ZT values are suppressed with increasing strength of interdot hopping processes. This is consisted with the study of quantum well superlattice, where the ZT is suppressed by decreasing the interwell distance.[2] It is noted that the tunneling rate should be affected due to the interdot hopping, and the ZT behavior should be altered as a consequence. However, the effect of interdot coupling on the tunneling rate is beyond the scope considered in the present paper.

So far, our discussion is limited to the linear-response regime with $\Delta T/T\ll 1$. Some functionalities of thermoelectric devices require that the applied temperature bias ΔT violates the $\Delta T/T\ll 1$ condition. In the following study, the thermoelectric properties of QD junctions are investigated in the nonlinear-response regime.

IV. NONLINEAR REGIME

Scheibner *et al.*[32] experimentally reported the thermal power of the two-dimensional (2D) electron gas in a QD system under high magnetic fields in the linear-response regime. Few theoretical works have reported the thermal properties of QD junctions in the nonlinear-response regime.[33] In Ref. 33, the thermal power in the Kondo regime based on the one-level Anderson model was studied theoretically. Here, we study the thermoelectric effect of multiple QD junction in the Coulomb-blockade effect in the nonlinear regime. We

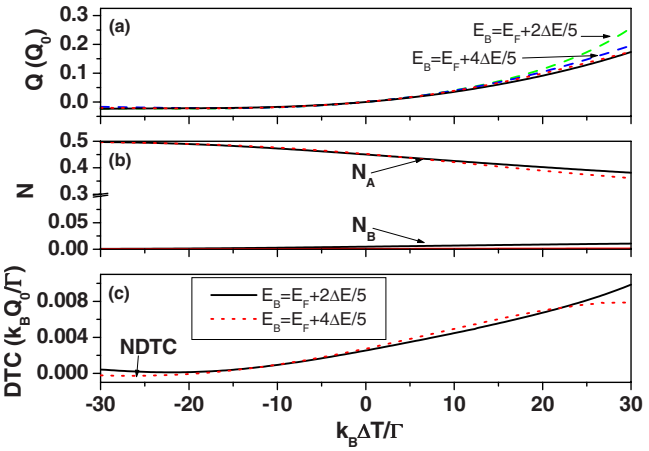

FIG. 9. (Color online) (a) Heat current Q (b) average occupation number N, and (c) DTC as a function of ΔT for various values of E_B for a two-QD junction. $\Gamma_{AR}=0$, $\eta_A=0.3$, and $\Delta E=200\Gamma$.

show that in the nonlinear regime, the thermal rectification behavior can become quite pronounced. Records of thermal rectification date back to 1935 when Starr discovered that copper oxide/copper junctions can display a thermal diode behavior.[34] Recently, thermal rectification effects have been predicted to occur in one-dimensional phonon junction systems.[35–39]

To study the direction-dependent heat current, we let $T_L=T_0+\Delta T/2$ and $T_R=T_0-\Delta T/2$, where $T_0=(T_L+T_R)/2$ is the equilibrium temperature of two side electrodes and $\Delta T=T_L-T_R$ is the temperature difference. Because the electrochemical potential difference, $e\Delta V$, yielded by the thermal gradient could be significant, it is important to keep track the shift of the energy level of each dot according to $\epsilon_\ell=E_\ell+\eta_\ell\Delta V/2$, where η_ℓ is the ratio of the distance between dot ℓ and the midplane of the QD junction to the junction width. Here we set $\eta_B=\eta_C=0$. A functional thermal rectifier requires a good thermal conductor for $\Delta T>0$ but a poor thermal conductor for $\Delta T<0$. Based on Eqs. (2) and (3), the asymmetrical behavior of heat current with respect to ΔT requires not only highly asymmetric coupling strengths between the QDs and the electrodes but also strong electron Coulomb interactions between dots. To investigate the thermal rectification behavior, we have numerically solved Eqs. (2) and (3) for multiple-QD junctions involving two QDs and three QDs for various system parameters. We first determine ΔV by solving Eq. (2) with $J_e=0$ (the open-circuit condition) for a given ΔT, T_0, and an initial guess of the average one-particle and two-particle occupancy numbers, N_ℓ and c_ℓ, for each QD. Those numbers are then updated according to Eqs. (5) and (6) until self-consistency is established. Once ΔV is solved, we then use Eq. (3) to compute the heat current.

Figure 9 shows the heat currents, occupation numbers, and differential thermal conductance (DTC) for the two-QD case, in which the energy levels of dot A and dot B are $E_A=E_F-\Delta E/5$ and $E_B=E_F+\alpha_B\Delta E$, where α_B is tuned between 0 and 1. We have adopted $\Delta E=200\Gamma$, which is used to describe the energy-level fluctuation of QDs. The heat currents are expressed in units of $Q_0=\Gamma^2/(2h)$ throughout this paper. The intradot and the interdot Coulomb interactions used are $U_\ell=30k_BT_0$ and $U_{AB}=15k_BT_0$. The tunneling rates are $\Gamma_{AR}=0$, $\Gamma_{AL}=2\Gamma$, and $\Gamma_{BR}=\Gamma_{BL}=\Gamma$. k_BT_0 is chosen to be 25Γ throughout this paper. Here, $\Gamma=(\Gamma_{AL}+\Gamma_{AR})/2$ is the average tunneling rate in energy units, whose typical values of interest are between 0.1 and 0.5 meV. The dashed curves are obtained by using a simplified expression of Eq. (3) in which we set the average two-particle occupation in dots A and B to zero (resulting from the large intradot Coulomb interactions) and taking the limit that $\Gamma \ll k_BT_0$ so the Lorentzian function of resonant channels can be replaced by a delta function. We have

$$Q/\gamma_B = \pi(1-N_B)[(1-2N_A)(E_B-E_F)f_{LR}(E_B) + 2N_A(E_B+U_{AB}-E_F)f_{LR}(E_B+U_{AB})]. \quad (13)$$

Here $N_{A(B)}$ is the average occupancy in dot A(B). Therefore, it is expected that the curve corresponding to $E_B=E_F+4\Delta E/5$ obtained with this delta function approximation is in good agreement with the full solution, since E_B is far away from the Fermi energy level. For cases when E_B is close to E_F, the approximation is not as good but it still gives qualitatively correct behavior. Thus, it is convenient to use this simple expression to illustrate the thermal rectification behavior. The asymmetrical behavior of N_A with respect to ΔT is mainly resulted from the conditions $\Gamma_{AR}=0$ and $\Gamma_{AL}=2\Gamma$. The heat current is contributed from the resonant channel with $\epsilon=E_B$ because the resonant channel with $\epsilon=E_B+U_{AB}$ is too high in energy compared with E_F. The sign of Q is determined by $f_{LR}(E_B)$, which indirectly depends on Coulomb interactions, tunneling-rate ratio, and QD energy levels. The rectification behavior of Q is dominated by the factor $1-2N_A$, which explains why the energy level of dot A should be chosen below E_F and the presence of interdot Coulomb interactions is crucial. The negative sign of Q in the regime of $\Delta T<0$ indicates that the heat current is from the right electrode to the left electrode. We define the rectification efficiency as $\eta_Q=[Q(+\Delta T)-|Q(-\Delta T)|]/Q(+\Delta T)$. We obtain $\eta_Q(\Delta T=30\Gamma)=0.86$ for $E_B=E_F+2\Delta E/5$ and $\eta_Q(\Delta T=30\Gamma)=0.88$ for $E_B=E_F+4\Delta E/5$. Figure 9(c) shows DTC in units of Q_0k_B/Γ. It is found that the rectification behavior is not very sensitive to the variation in E_B. DTC is roughly linearly proportional to ΔT in the range $-20\Gamma<k_B\Delta T<20\Gamma$. In addition, we also find a small negative DTC (NDTC) for $E_B=E_F+4\Delta E/5$. Similar behavior was reported in the phonon junction system.[40]

Note that the mechanism of thermal rectification is similar to the charge-current rectification. However, the heat current is yielded by the temperature bias and the electrochemical potential. In particular, the electrochemical potential is a highly nonlinear function of the temperature bias, which has never been reported for quantum dot junctions. Consequently, it is not straightforward to reveal the behavior of heat current with respect to the temperature bias. The manifested difference between the heat current and the charge current is that the origin of NDTC is different from that of negative differential conductance (NDC). The NDC of charge current requires the upper energy levels with the shell-filling condition, which was discussed in Refs. 18 and 19. For NDTC, it only appears in the lower level with shell-

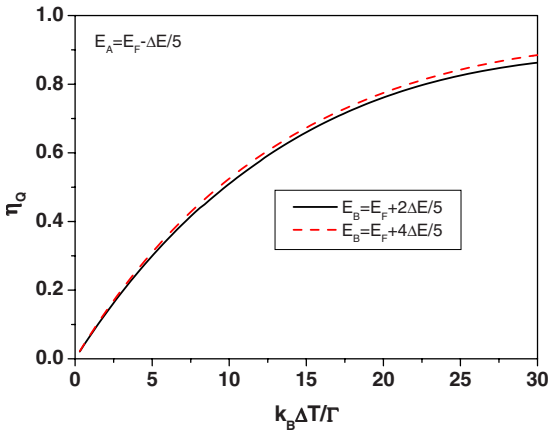

FIG. 10. (Color online) Rectification efficiency (η_Q) as a function of ΔT for two different values of E_B. Other parameters are the same as those for Fig. 9.

filling condition. Figure 10 shows the rectification efficiency as a function ΔT for two different values of E_B. The rectification efficiency vanishes when $k_B\Delta T/\Gamma \ll 1$. This implies that it is difficult to judge the rectification effect in the linear-response regime of $\Delta T/T_0 \ll 1$. Although the two-dot case can reach a high-rectification efficiency, the heat current should be enhanced from the application point of view.

Figure 11 shows the heat current, differential thermal conductance, and thermal power as functions of temperature difference ΔT for a three-QD case for various values of Γ_{AR} while keeping $\Gamma_{B(C),R}=\Gamma_{B(C),L}=\Gamma$. Here, we adopt $\eta_A=|\Gamma_{AL}-\Gamma_{AR}|/(2\Gamma)$ instead of fixing η_A at 0.3 to reflect the correlation of dot position with the asymmetric tunneling rates. We assume that the three QDs are roughly aligned with dot A in the middle. The energy levels of dots A, B, and C are chosen to be $E_A=E_F-\Delta E/5$, $E_B=E_F+2\Delta E/5$, and $E_C=E_F+3\Delta E/5$. $U_{AC}=U_{BA}=15k_BT_0$, $U_{BC}=8k_BT_0$, $U_C=30k_BT_0$, and all other parameters are kept the same as in the two-dot case. The thermal rectification effect is most pronounced when $\Gamma_{AR}=0$, as seen in Fig. 12(a). (Note that the heat current is not very sensitive to U_{BC}). In this case, we obtain a small heat

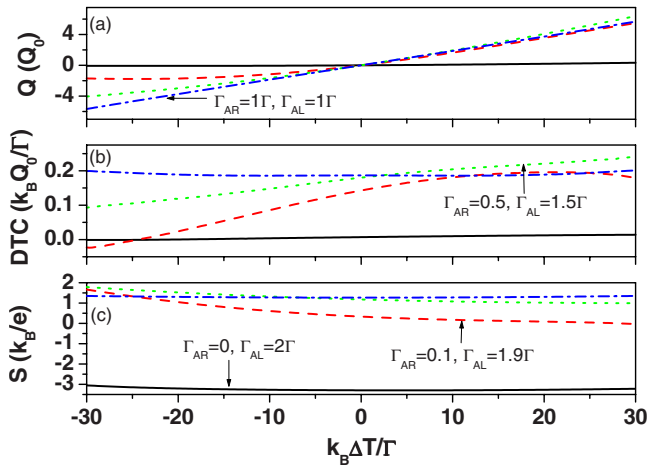

FIG. 11. (Color online) (a) Heat current Q, (b) DTC, and (c) thermal power S as a function of ΔT for various values of Γ_{AR} for a three-QD junction.

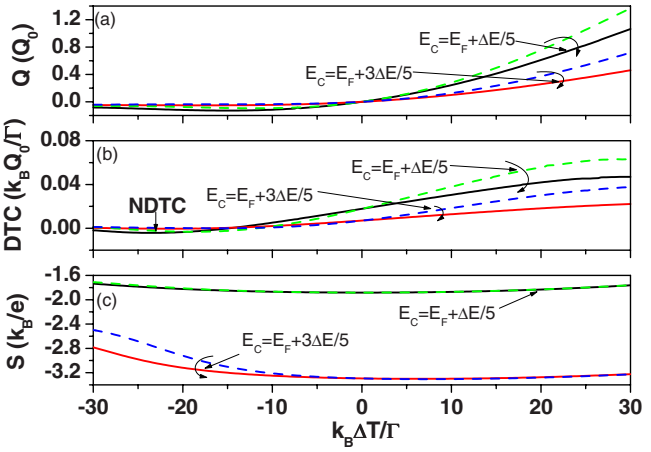

FIG. 12. (Color online) (a) Heat current Q, (b) DTC, and (c) thermal power S as functions of ΔT for various values of E_C for a three-QD junction with $\Gamma_{AR}=0$ and $\eta_A=0.3$.

current $Q=0.068Q_0$ at $\Delta T=-30\Gamma$ but a large heat current $Q=0.33Q_0$ at $\Delta T=30\Gamma$ and the rectification efficiency η_Q is 0.79. However, the heat current for $\Gamma_{AR}=0$ is small. For $\Gamma_{AR}=0.1\Gamma$, we obtain $Q=1.69Q_0$ at $\Delta T=-30\Gamma$, $Q=5.69Q_0$ at $\Delta T=30\Gamma$, and $\eta_Q=0.69$. We see that the heat current is suppressed for $\Delta T<0$ with decreasing Γ_{AR}. This implies that it is important to blockade the heat current through dot A to observe the rectification effect. Very clear NDTC is observed in Fig. 11(b) for the $\Gamma_{AR}=0.1\Gamma$ case while DTC is symmetric with respect to ΔT for the $\Gamma_{AR}=\Gamma_{AL}$ case.

From the experimental point of view, it is easier to measure the thermal power than the direction-dependent heat current. The thermal power as a function of ΔT is shown in Fig. 11(c). All curves except the dashed-dotted line (which is for the symmetrical tunneling case) show highly asymmetrical behavior with respect to ΔT, yet it is not easy at all to judge the efficiency of the rectification effect from S for small $|\Delta T|$ ($k_B|\Delta T|/\Gamma<10$). Thus, it is not sufficient to determine whether a single QD can act as an efficient thermal rectifier based on results obtained in the linear-response regime of $\Delta T/T_0 \ll 1$.[32] According to the thermal-power values, the electrochemical potential $e\Delta V$ can be very large. Consequently, the shift of QD energy levels caused by ΔV is quite important. To illustrate the importance of this effect, we plot in Fig. 12 the heat current for various values of E_C for the case with $\Gamma_{AR}=0$, $U_{BC}=10k_BT_0$, and $\eta_A=0.3$. Other parameters are kept the same as those for Fig. 11. The solid (dashed) curves are obtained by including (excluding) the energy shift $\eta_A\Delta V/2$. It is seen that the shift of QD energy levels due to ΔV can lead to significant change in the heat current. It is found that NDTC is accompanied with low heat current for the case of $E_C=E_F+\Delta E/5$ [see Fig. 12(b)]. Even though the heat current exhibits rectification effect for $E_C=E_F+\Delta E/5$ and $E_C=E_F+3\Delta E/5$, the thermal power has a very different behavior. From Figs. 11(c) and 12(c), we see that the heat current is a highly nonlinear function of electrochemical potential, ΔV. Consequently, the rectification effect is not straightforwardly related to the thermal power in this system.

Because the position distribution fluctuation is common for QDs, we investigate the interdot Coulomb interactions on

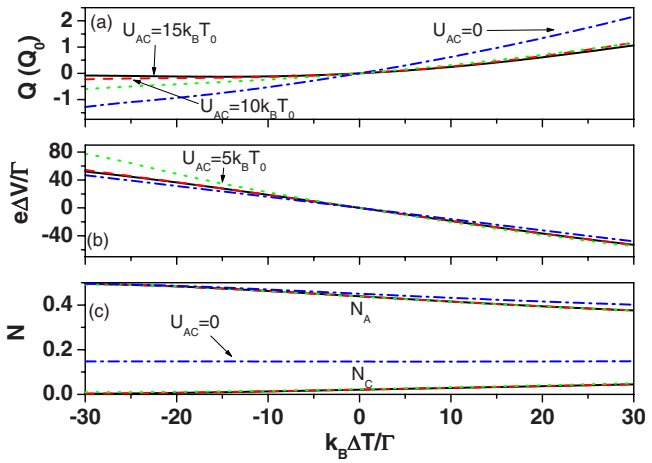

FIG. 13. (Color online) (a) Heat current Q, (b) electrochemical potential, $e\Delta V$, and (c) occupation number N functions of ΔT for various values of U_{AC} for a three-QD junction with $E_C=E_F+\Delta E/5$. All other parameters are the same as for Fig. 12.

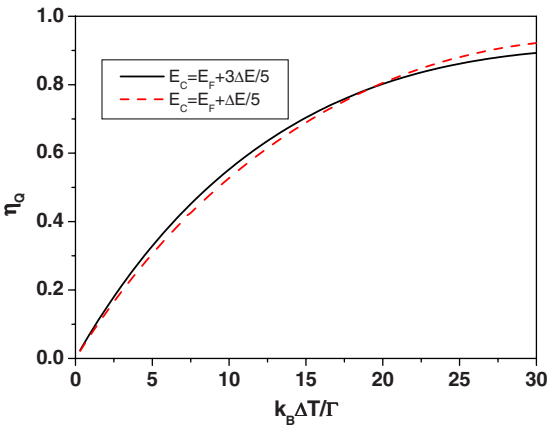

FIG. 14. (Color online) Rectification efficiency (η_Q) as a function of ΔT for two different values of E_C. Other parameters are the same as those for Fig. 12.

the rectification effect. Figure 13 shows the heat current, electrochemical potential, and occupation number as functions of ΔT for various values of U_{AC} with $E_C=E_F+\Delta E/5$. Other parameters are the same as in Fig. 12. When $U_{AC}=0$, the rectification efficiency is suppressed seriously. The residue rectification mainly arises from the correlation between dot A and dot B. Such results indicate that it is crucial to control the QD position in the implementation of QD thermal rectifiers. We find that the electrochemical potential is not significantly changed when U_{AC} decreases whereas the heat current has a considerable variation. Figure 13(c) shows the occupation numbers of dots A and C. N_B are ignored due to their energy levels being far away from the Fermi energy level. It is expected that N_A is not sensitive to the decrease in U_{AC}. N_C increases so much when U_{AC} decreases since the main resonant channels of dot C are dominated by E_C rather than the combination of E_C and E_C+U_{AC}. Figure 13(c) reveals that the serious suppression of rectification efficiency of dotted-dashed line shown in Fig. 13(a) is mainly attributed to the heat current through dot C. We once again investigate the rectification efficiency for three-dot case. Figure 14 shows the rectification efficiency as function of ΔT. All other parameters are the same as those of Fig. 12. The rectification efficiency increases with increasing temperature bias. However, η_Q is not sensitive to the energy level of dot C.

Comparing the heat current of the three-dot case (shown in Figs. 11 and 12) to the two-dot case (shown in Fig. 9), we find that the rectification efficiency is about the same for both cases (shown in Figs. 10 and 14), while the magnitude of the heat current can be significantly enhanced in the three-dot case. For practical applications, we need to estimate the magnitude of the heat-current density and DTC of the insulator/quantum dots/vacuum (IQV) junction device in order to see if the effect is significant. We envision a thermal rectification device made of an array of multiple QDs (e.g., three-QD cells) with a 2D density $N_{\mathrm{QD}}=10^{11}$ cm^{-2}. For this device, the heat-current density versus ΔT is given by Figs. 11 and 12 with the units Q_0 replaced by $N_{\mathrm{QD}}Q_0$, which is approximately 965 W/m^2 if we assume $\Gamma=0.5$ meV. Similarly, the units for DTC become $N_{2d}k_BQ_0/\Gamma$, which is approximately 34 W/K m^2. Since the phonon contribution can be blocked by the vacuum layer in our design, this device could have practical applications near 140 K with ($k_BT_0\approx 12.5$ meV). If we choose a higher tunneling rate $\Gamma>1$ meV and Coulomb energy >300 meV (possible for QDs with diameter less than 1 nm), then it is possible to achieve room-temperature operation. It is worth pointing out that if the vacuum layer is replaced by a typical phonon glass, such as SiO_2, which has a thermal conductivity of $C_{ph}=1.5$ W/K m (Ref. 41) at room temperature, the heat current carried by phonons across a 10 nm junction with a temperature bias of 1 K would be around 1.5×10^8 W/m^2. This would completely dominate over the thermoelectric effect considered here (by six orders of magnitude). Therefore, unless a vacuum layer is inserted, the phonon thermal conductance, κ_{ph}, will play a dominant role.

V. SUMMARY AND CONCLUSIONS

We have theoretically investigated the effect of intradot and interdot Coulomb interactions on the figure of merit (ZT) and thermal power (S) of multiple QD junction system in the sequential tunneling process. It is found that the ZT values at high temperatures are significantly suppressed by the intradot as well as the interdot Coulomb interactions. The optimization of ZT depends not only on temperature but also on the detuning energy ($\Delta=E_g-E_F$). It is worth noting that inelastic scattering effect arising from QD-size fluctuations, defects, and electron-phonon interactions would also lead to considerable reduction to the ZT values. We also found that the electrical conductance and thermal power exhibit Coulomb oscillatory behavior and the sawtoothlike behavior with respect to the gate voltage. The largest value for ZT is obtained midway between good and poor conductors. Apart from the results of linear response, the heat-rectification effect can be observed for multiple QD junctions in the nonlinear-response regime. In contrast to the heat rectification of phonon junction system, the heat current is carried by electrons in the multiple QD junction system and large electrochemical po-

tentials can be established by the temperature gradient to generate electrical power. We have suggested a way to fabricate a vacuum barrier that is thin enough to allow for electron tunneling, although it may be technologically challenging. Such a technology of fabricating vacuum layer would also be very useful in realizing quantum tunneling devices such as molecular transistors in which it is critical to eliminate the effect due to ambient molecules.[42] Finally, we note that it is possible to perform a single-QD heat-tunneling measurements under high vacuum by using a scanning tunneling-microscope (STM) setup to investigate the contribution of QD tunneling mechanism to the thermoelectric effect.[43] Since a vacuum gap between the QD and the metallic STM tip is already present in the setup, the phonon heat conduction is blocked, the STM setup satisfies the condition specified in our Fig. 1 and it can be used to verify our theoretical predictions.

ACKNOWLEDGMENTS

This work was supported in part by the National Science Council of the Republic of China under Contracts No. NSC 97-2112-M-008-017-MY2 and No. NSC 98-2112-M-001-022-MY3 and by Academia Sinica.

*mtkuo@ee.ncu.edu.tw
†yiachang@gate.sinica.edu.tw

[1] A. J. Minnich, M. S. Dresselhaus, Z. F. Ren, and G. Chen, Energy Environ. Sci. **2**, 466 (2009).
[2] G. Mahan, B. Sales, and J. Sharp, Phys. Today **50**(3), 42 (1997).
[3] R. Venkatasubramanian, E. Siivola, T. Colpitts, and B. O'Quinn, Nature (London) **413**, 597 (2001).
[4] A. I. Boukai, Y. Bunimovich, J. Tahir-Kheli, J. K. Yu, W. A. Goddard III, and J. R. Heath, Nature (London) **451**, 168 (2008).
[5] T. C. Harman, P. J. Taylor, M. P. Walsh, and B. E. LaForge, Science **297**, 2229 (2002).
[6] K. F. Hsu, S. Loo, F. Guo, W. Chen, J. S. Dyck, C. Uher, T. Hogan, E. K. Polychroniadis, and M. G. Kanatzidis, Science **303**, 818 (2004).
[7] A. Majumdar, Science **303**, 777 (2004).
[8] G. Chen, M. S. Dresselhaus, G. Dresselhaus, J. P. Fleurial, and T. Caillat, Int. Mater. Rev. **48**, 45 (2003).
[9] Y. M. Lin and M. S. Dresselhaus, Phys. Rev. B **68**, 075304 (2003).
[10] P. Murphy, S. Mukerjee, and J. Moore, Phys. Rev. B **78**, 161406(R) (2008).
[11] N. S. Wingreen, K. W. Jacobsen, and J. W. Wilkins, Phys. Rev. B **40**, 11834 (1989).
[12] A. P. Jauho, N. S. Wingreen, and Y. Meir, Phys. Rev. B **50**, 5528 (1994).
[13] David M.-T. Kuo and Y. C. Chang, Phys. Rev. B **66**, 085311 (2002).
[14] U. Lundin and R. H. McKenzie, Phys. Rev. B **66**, 075303 (2002).
[15] K. Flensberg, Phys. Rev. B **68**, 205323 (2003).
[16] Z. Z. Chen, R. Lu, and B. F. Zhu, Phys. Rev. B **71**, 165324 (2005).
[17] M. Galperin, A. Nitzan, and M. A. Ratner, Phys. Rev. B **75**, 155312 (2007).
[18] David M.-T. Kuo and Y. C. Chang, Phys. Rev. Lett. **99**, 086803 (2007).
[19] Y. C. Chang and David M.-T. Kuo, Phys. Rev. B **77**, 245412 (2008).
[20] L. A. Wu and D. Segal, Phys. Rev. Lett. **102**, 095503 (2009).
[21] O. P. Saira, M. Meschke, F. Giazotto, A. M. Savin, M. Möttönen, and J. P. Pekola, Phys. Rev. Lett. **99**, 027203 (2007).
[22] H. Haug and A. P. Jauho, *Quantum Kinetics in Transport and Optics of Semiconductors* (Springer, Heidelberg, 1996).
[23] S. Datta, *Electronic Transport in Mesoscopic Systems* (Cambridge University Press, Cambridge, U.K., 1995).
[24] R. Scheibner, E. G. Novik, T. Borzenko, M. Konig, D. Reuter, A. D. Wieck, H. Buhmann, and L. W. Molenkamp, Phys. Rev. B **75**, 041301(R) (2007).
[25] X. Zianni, Phys. Rev. B **78**, 165327 (2008).
[26] C. W. J. Beenakker, Phys. Rev. B **44**, 1646 (1991).
[27] R. Scheibner, H. Buhmann, D. Reuter, M. N. Kiselev, and L. W. Molenkamp, Phys. Rev. Lett. **95**, 176602 (2005).
[28] K. A. Matveev and A. V. Andreev, Phys. Rev. B **66**, 045301 (2002).
[29] T. Markussen, A. P. Jauho, and M. Brandbyge, Phys. Rev. Lett. **103**, 055502 (2009).
[30] T. Markussen, A. P. Jauho, and M. Brandbyge, Phys. Rev. B **79**, 035415 (2009).
[31] G. Chen, *Nanoscale Energy Transport and Conversion* (Oxford University Press, New York, 2005).
[32] R. Scheibner, M. Konig, D. Reuter, A. D. Wieck, C. Gould, H. Buhmann, and L. W. Molenkamp, New J. Phys. **10**, 083016 (2008).
[33] M. Krawiec and K. I. Wysokinski, Phys. Rev. B **75**, 155330 (2007).
[34] C. Starr, J. Appl. Phys. **7**, 15 (1936).
[35] M. Terraneo, M. Peyrard, and G. Casati, Phys. Rev. Lett. **88**, 094302 (2002).
[36] B. Li, L. Wang, and G. Casati, Phys. Rev. Lett. **93**, 184301 (2004).
[37] B. Hu, L. Yang, and Y. Zhang, Phys. Rev. Lett. **97**, 124302 (2006).
[38] G. Casati, C. Mejia-Monasterio, and T. Prosen, Phys. Rev. Lett. **98**, 104302 (2007).
[39] N. Zeng and J. S. Wang, Phys. Rev. B **78**, 024305 (2008).
[40] D. Segal, Phys. Rev. B **73**, 205415 (2006).
[41] D. G. Cahill and R. O. Pohl, Phys. Rev. B **35**, 4067 (1987).
[42] J. Taylor, H. Guo, and J. Wang, Phys. Rev. B **63**, 245407 (2001).
[43] N. D. Lang, Phys. Rev. B **45**, 13599 (1992).